

Effect of Orientation on the Free Volume and Oxygen Transport of a Polypropylene Copolymer

L. S. SOMLAI,^{1,*} R. Y. F. LIU,^{1,†} L. M. LANDOLL,^{2,‡} A. HILTNER,¹ E. BAER¹

¹Department of Macromolecular Science, Center for Applied Polymer Research, Case Western Reserve University, Cleveland, Ohio 44106-7202

²Applied Extrusion Technologies, New Castle, Delaware 19720

Received 5 November 2004; revised 5 January 2005; accepted 7 January 2005

DOI: 10.1002/polb.20412

Published online in Wiley InterScience (www.interscience.wiley.com).

ABSTRACT: The effect of uniaxial orientation on the free-volume and oxygen-transport properties of a propylene copolymer with 4.5 wt % ethylene was examined. The free-volume hole size and hole density were measured with positron annihilation lifetime spectroscopy. Subsequently, the free-volume characteristics were correlated with the oxygen-transport properties. Orientation had only a small effect on the total amount of free volume: a small increase in the hole density was offset by a small decrease in the hole size. As a result, the oxygen solubility and amorphous-phase density were unchanged by orientation. However, a pronounced decrease in the oxygen diffusivity when the draw ratio exceeded 6 indicated a change in the dynamic free volume. This was attributed to an increasing number of taut tie chains, which retarded oxygen diffusion. The reduced amorphous chain mobility was also manifest in the increased glass-transition temperature, decreased bulk thermal expansivity, and decreased expansivity of free-volume holes. ©2005 Wiley Periodicals, Inc. *J Polym Sci Part B: Polym Phys* 43: 1230–1243, 2005

Keywords: diffusion; free volume; orientation; oxygen transport; permeability; poly(propylene) (PP); solubility

INTRODUCTION

Atmosphere control is extremely important to the beverage and food packaging industries and is dependent on the gas-transport properties of polymer films.¹ Polypropylene is a candidate material for packaging applications because of its low cost and good thermal stability in comparison with polyethylene. Commercial polypropylene films are typically oriented by a tentering process in which an extruded film is quenched, reheated, and biaxially drawn into a film.^{2,3} Orientation improves

both the mechanical and gas-barrier properties of the films.^{4–6} To achieve appropriate atmosphere control, a fundamental understanding of gas transport, including the effect of orientation, is required.

The orientation of amorphous polymers such as poly(ethylene terephthalate) can significantly enhance barrier properties.^{7–9} The free volume can be noticeably reduced by orientation through cold drawing even though crystallization is prevented. As a result, the amorphous glass is densified with a proportional decrease in the oxygen solubility. Drawing a semicrystalline polymer such as polypropylene, however, results in a structural transformation of spherulites into microfibrils. An improvement in properties such as the axial elastic modulus and sonic modulus upon stretching is ascribed to taut tie molecules, which

*Present address: Baxter Healthcare, Cleveland, Mississippi, 38732

†Present address: 3M, St. Paul, Minnesota, 55144

‡Correspondence to: A. Hiltner (E-mail: pah6@po.cwru.edu)

Journal of Polymer Science: Part B: Polymer Physics, Vol. 43, 1230–1243 (2005)
©2005 Wiley Periodicals, Inc.

interconnect crystalline blocks of the same or different microfibrils.^{10,11} Because gas transport only occurs in the amorphous phase of polypropylene, tie molecules are expected to be important in the resulting gas-transport properties of drawn films. Indeed, a significant reduction in the permeability when the draw ratio (λ) exceeds 6 suggests that taut tie molecules act as effective obstacles to penetrant molecules.¹¹ However, the relationship of the orientation in general and taut tie molecules in particular with the free-volume structure of the amorphous phase is not well understood.

It is the purpose of this article to provide further insight into gas transport through oriented films of a propylene copolymer. Oxygen-transport properties are studied in combination with other solid-state characterization methods of birefringence and thermal expansion. The nature of the free volume is probed directly by positron annihilation lifetime spectroscopy (PALS). The results are analyzed in terms of free-volume concepts of gas transport.

EXPERIMENTAL

The propylene-ethylene copolymer with 4.5 wt % ethylene (EP4.5) was provided by Atofina; it had a density of 0.895 g cm^{-3} (ASTM D 1505) and a melt flow index of 6.8 g/10 min (ASTM D 1238).

Films of various thicknesses between 110 and 1700 μm were prepared by melt extrusion. The temperature of the melt was 210 °C, and the films were taken up from the film die onto a chill roll. Specimens cut from the films were stretched under constrained uniaxial conditions.⁷ The specimen width before stretching was 150 mm, and the thickness and gauge length were varied to achieve a final thickness of 100–200 μm . Each specimen was clamped between wide grips, mounted in the environmental chamber of an Instron machine, preheated at 128 °C for 15 min, and subsequently drawn at a rate of $10,000\% \text{ min}^{-1}$ to the target λ value. To obtain barrier specimens that differed in λ but had about the same thickness, we used thinner films and larger gauge lengths for lower λ values; thicker films and smaller gauge lengths were required for higher λ values. For example, an EP4.5 specimen 900 μm thick with a gauge length of 30 mm was used to obtain a barrier specimen with a λ value of about 6, whereas a specimen 1600 μm thick with a gauge length of 20 mm was used to obtain a barrier specimen with a λ value of about 12. After being drawn, each film

was rapidly cooled to the ambient temperature in the grips by the opening of the door of the environmental chamber. λ was determined from the cross-head displacement and confirmed with ink markings on the specimen. A 190- μm -thick unoriented heat-set control film was also prepared with the same preheating and cooling procedure without stretching.

The refractive index at a wavelength of 633 nm was measured with a Metricon 2010 prism coupler. The refractive index was measured in-plane parallel and transverse to the stretch direction and in the normal or thickness direction. Five points spread across each specimen were measured, and the average values are reported. The standard deviation, which was typically less than 0.0004, indicated good homogeneity in the specimens.

The density was measured with a density gradient column constructed from 2-propanol and deionized water in accordance with ASTM D 1505 method B. The column was calibrated with glass floats of known density. Small pieces of film ($\sim 25 \text{ mm}^2$) were placed in the column and allowed to equilibrate for 30 min before the measurements were taken. The standard deviation was within $\pm 0.0005 \text{ g cm}^{-3}$ for four specimens. The temperature of the density column was varied from 5 to 40 °C ($\pm 0.1 \text{ °C}$) in 5 °C increments with a Thermo-Neslab thermal bath. Density measurements were taken 30 min after the column temperature had stabilized.

Thermograms were obtained with a PerkinElmer DSC-7 at a heating rate of 10 °C min^{-1} over a temperature range of -60 to 190 °C . The melting enthalpy (ΔH_m) was taken from the initial heating thermogram.

The oxygen flux at 0% relative humidity, 1 atm of pressure, and temperatures ranging from -35 to $+45 \text{ °C}$ ($\pm 0.1 \text{ °C}$) was measured with a Mocon Ox-Tran 2/20 fitted with a remote diffusion cell and a Thermo-Neslab thermal bath. The instrument was calibrated at 23 °C with NIST-certified Mylar films of known transport characteristics. To obtain accurate permeability, $P = Jl/p$, where p is the oxygen pressure and J is the oxygen flux, we determined the average thickness (l) of each film as $l = W(A\rho)^{-1}$, where W is the specimen weight, A is the specimen area, and ρ is the density. The error in determining the permeability was estimated not to exceed 3%.

For the steady-state oxygen flux through thin, highly permeable EP4.5 films not to exceed the Mocon detector range, the oxygen pressure in the permeant stream was sometimes reduced

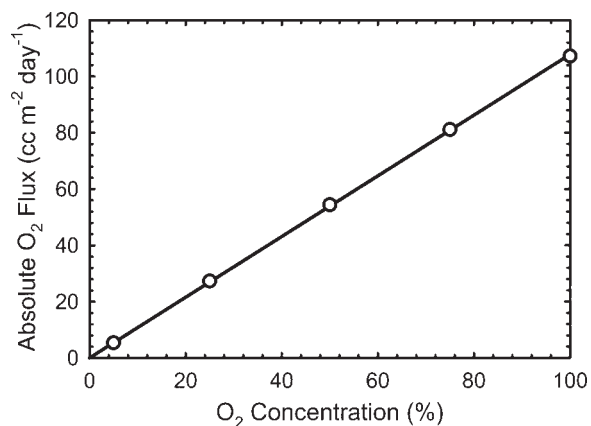


Figure 1. Linear relationship between the oxygen permeability and the oxygen concentration for a 12- μm -thick Mylar calibration film.

via mixing with nitrogen. Figure 1 shows the linear relationship with correlation coefficient $r^2 = 0.999$ between the oxygen concentration and absolute oxygen flux through a 12- μm -thick Mylar film at 23 °C.

PALS was performed from -80 to $+90$ °C with a conventional fast-fast coincidence system. The instrumentation and procedures for data analysis were described previously.¹² Ten spectra were collected for each specimen, and the standard deviation of the calculated hole radius was within ± 0.01 Å.

RESULTS

Orientation

The physical properties of the unoriented films are summarized in Table 1. Differences in the process conditions resulted in slight variations in

the extruded film density. Heat setting increased the density of a 190- μm -film from 0.8989 to about 0.8999 g cm^{-3} . The volume crystallinity from the density ($\phi_{c,\rho}$) can be calculated as follows:

$$\phi_{c,\rho} = \frac{\rho - \rho_a}{\rho_c - \rho_a} \quad (1)$$

where ρ , ρ_a , and ρ_c are the bulk density, amorphous-phase density (0.853 g cm^{-3}), and crystalline phase density (0.936 g cm^{-3}), respectively.¹³ $\phi_{c,\rho}$ was 0.52, 0.55, 0.57, and 0.53 for 640- μm , 190- μm , 190- μm heat-set, and 110- μm films, respectively. The volume crystallinity (ϕ_c) was also determined from the differential scanning calorimetry (DSC) heat of melting (ΔH_m):

$$\phi_c = \frac{\Delta H_m}{\Delta H_0} \left(\frac{\rho}{\rho_c} \right) \quad (2)$$

where ΔH_0 (the heat of melting of the crystal) is 209 J mol^{-1} .^{14,15} ϕ_c from DSC was 0.39–0.42, significantly lower than $\phi_{c,\rho}$ (Table 1). The discrepancy has been attributed to the existence of an interphase.¹⁶ An alternative explanation is that the value taken for ρ_a in eq 1 is not reliable. To obtain a crystallinity from density comparable to the crystallinity from the heat of melting requires a value of 0.869 g cm^{-3} for ρ_a , which is not unreasonable.

Stretching EP4.5 films under the constrained uniaxial conditions used in this study resulted in neck formation and propagation, followed by uniform strain hardening. The natural draw ratio value of EP4.5 was about 5.5, similar to that of polypropylene.¹⁷ Uniformly oriented films were obtained through stretching to various λ values in the strain-hardening region. λ values in the

Table 1. Physical Properties of Unoriented EP4.5 Films

Thickness (μm)	ρ at 23 °C (g cm^{-3})	$\phi_{c,\rho}$ (vol%)	ΔH_m (J/g)	ϕ_c (vol%)	T (°C)	P^a	$D(10^{-13})^b$	S^c
640	0.8958	0.52	88	0.40	23	9.15	159	0.067
190	0.8989	0.55	85	0.39	–30	0.342	3.76	0.105
					23	9.20	—	—
190 ^d	0.8999	0.57	90	0.42	–30	0.457	4.20	0.126
					23	9.93	—	—
110	0.8973	0.53	86	0.39	–30	0.448	4.50	0.115
					23	8.72	—	—
					–30	0.358	2.56	0.162

^a cc[STP] $\text{cm m}^{-2} \text{day}^{-1} \text{atm}^{-1}$

^b $\text{m}^2 \text{s}^{-1}$

^c $\text{cc cm}^{-3} \text{atm}^{-1}$

^d Heat-set (hs).

Table 2. Physical Properties of Oriented EP4.5 Films

λ	Thickness (μm)	ρ at 23°C (g cm^{-3})	$\phi_{c,\rho}$ (vol %)	ϕ_c (vol %)	Δn	T (°C)	P^a	D (10^{-13}) ^b	S^c
1.0	190 ^d	0.8999	0.57	0.42	0	23	9.93	—	—
						−30	0.448	4.50	0.115
6.2	140	0.9003	0.57	0.38	0.0205	23	9.11	—	—
						−30	0.490	4.76	0.119
6.8	210	0.8996	0.56	—	0.0219	23	9.14	—	—
						−30	—	—	—
8.4	180	0.8999	0.56	0.48	0.0263	23	7.37	—	—
						−30	0.428	4.55	0.109
9.3	110	0.9003	0.57	—	0.0273	23	6.31	—	—
						−30	—	—	—
10.2	150	0.8998	0.56	0.45	0.0288	23	5.20	—	—
						−30	0.332	3.20	0.120
11.0	150	0.9001	0.57	—	0.0299	23	4.59	—	—
						−30	—	—	—
12.5	110	0.9003	0.57	0.44	0.0301	23	3.40	—	—
						−30	0.245	2.14	0.132

^a cc[STP] $\text{cm m}^{-2} \text{day}^{-1} \text{atm}^{-1}$

^b $\text{m}^2 \text{s}^{-1}$

^c $\text{cc cm}^{-3} \text{atm}^{-1}$

^d Heat-set (hs).

range of roughly 6–12 were obtained by this method. Orientation did not significantly change the density with respect to the density of the 190- μm heat-set control film (Table 2). Despite the discrepancy between the crystallinity from density and the crystallinity from DSC, both methods showed that ϕ_c was not altered to any significant degree by orientation. The stretched films remained clear with no stress whitening, and this indicated the absence of microvoiding.¹⁸

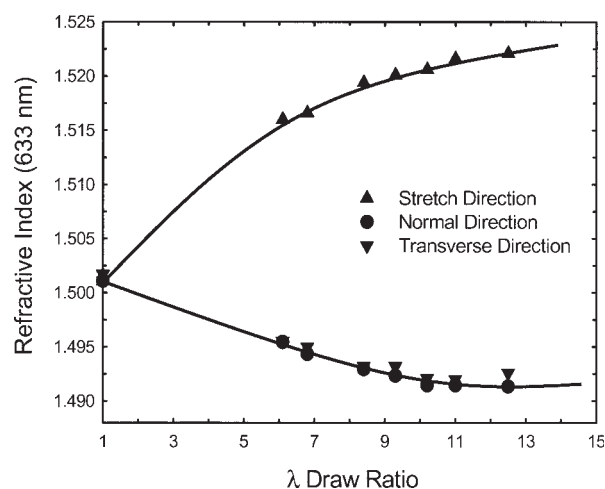
The refractive index in three directions as a function of λ is plotted in Figure 2. In the stretch direction, the refractive index continuously increased with gradually decreasing slope. On the other hand, in both the transverse and normal directions, the refractive index gradually decreased to a λ value of about 10, leveling off at a higher λ value. From the refractive index, the birefringence (Δn) can be readily calculated as follows:⁴

$$\Delta n = n_S - \frac{n_T + n_N}{2} \quad (3)$$

where n_S , n_T , and n_N are the refractive indices in the stretch, transverse, and normal directions. The Δn values of oriented EP4.5 films are included in Table 2.

Similar relationships between Δn and λ were observed in isotactic polypropylene films stretched at 110 and 135 °C.¹⁹ The separation of Δn into

crystalline and amorphous contributions indicated that the crystalline birefringence increased more rapidly at lower orientation ($\lambda < 6$) than the amorphous birefringence, whereas at a higher orientation ($\lambda > 6$), the crystalline birefringence leveled off. It was suggested that continuously increasing amorphous birefringence was mainly responsible for the increase in Δn at higher λ values.¹⁹ On the basis of previous studies, it appears that increases in Δn of EP4.5 films with λ values of 6–12 result mainly from the increasing orientation of the amorphous phase.

**Figure 2.** Refractive index as a function of λ .

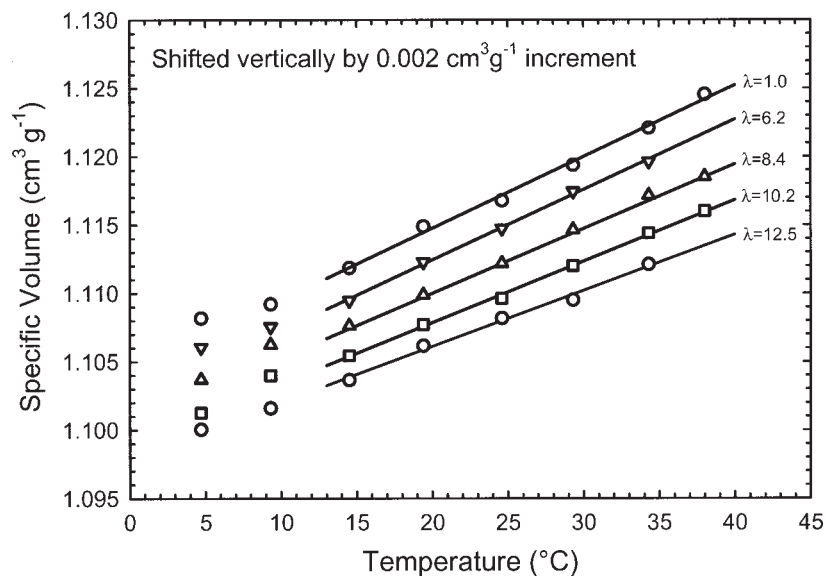


Figure 3. Temperature dependence of the bulk specific volume of oriented EP4.5. The curves are shifted vertically by $0.002 \text{ cm}^3 \text{ g}^{-1}$ increments.

Free-Volume Structure

Figure 3 shows the specific volume ($v = 1/\rho$) of EP4.5 films oriented to different λ values as a function of temperature. Because orientation had a very small effect on the absolute value of v , the data have been shifted for clarity. Above the glass-transition temperature (T_g), v increased linearly with temperature. The slope obtained from

the linear fit represented the bulk thermal expansivity above T_g ($\alpha_{b,1}$; Table 3). The thermal expansivity of the $190\text{-}\mu\text{m}$ heat-set film ($5.2 \times 10^{-4} \text{ cm}^3 \text{ g}^{-1} \text{ K}^{-1}$) was slightly lower than that reported for isotactic polypropylene ($5.5 \times 10^{-4} \text{ cm}^3 \text{ g}^{-1} \text{ K}^{-1}$).²⁰ The bulk thermal expansivity decreased with λ , from $5.2 \times 10^{-4} \text{ cm}^3 \text{ g}^{-1} \text{ K}^{-1}$ for $\lambda = 1.0$ to $4.3 \times 10^{-4} \text{ cm}^3 \text{ g}^{-1} \text{ K}^{-1}$ for $\lambda = 12.5$. Because the crys-

Table 3. Summary of Thermal Expansion Coefficients and PALS Results

Property	λ				
	1.0(heat-set)	6.2	8.4	10.2	12.5
$\alpha_{b,1}$ ($10^{-4} \text{ cm}^3 \text{ g}^{-1} \text{ K}^{-1}$)	5.2	5.1	4.6	4.5	4.3
$\alpha_{a,1}$ ($10^{-4} \text{ cm}^3 \text{ g}^{-1} \text{ K}^{-1}$)	7.5	6.9	6.8	6.4	5.9
T_g ($\text{O}_2 P$, $^{\circ}\text{C}$)	-7	-7	-5	1	4
T_g (PALS, $^{\circ}\text{C}$)	5	7	11	11	12
$\alpha_{h,g}$ ($\text{\AA}^3 \text{ K}^{-1}$) ^a	0.27	0.28	0.23	0.22	0.20
$\langle v_h \rangle$ at -30°C (\AA^3)	72	73	73	71	70
$\alpha_{h,1}$ ($\text{\AA}^3 \text{ K}^{-1}$) ^b	1.46	1.37	1.22	1.14	1.04
$\langle v_h \rangle$ at 80°C (\AA^3)	189	183	166	158	150
N_h (10^{20} g^{-1})	5.1	5.3	5.4	5.4	5.6
N_h at -30°C (10^{20} cm^{-3})	4.5	4.7	4.8	4.8	5.0
FFV at 23°C	0.049	0.050	0.047	0.046	0.045
FFV at -30°C	0.033	0.034	0.035	0.034	0.035
S_a at -30°C	0.20	0.19	0.21	0.22	0.24
T_2 ($^{\circ}\text{C}$)	-52	-50	-57	-59	-61
$T_g - T_2$ ($^{\circ}\text{C}$)	57	57	68	70	73

^a Thermal expansivity of free-volume holes in the amorphous phase below T_g .

^b Thermal expansivity of free-volume holes in the amorphous phase above T_g .

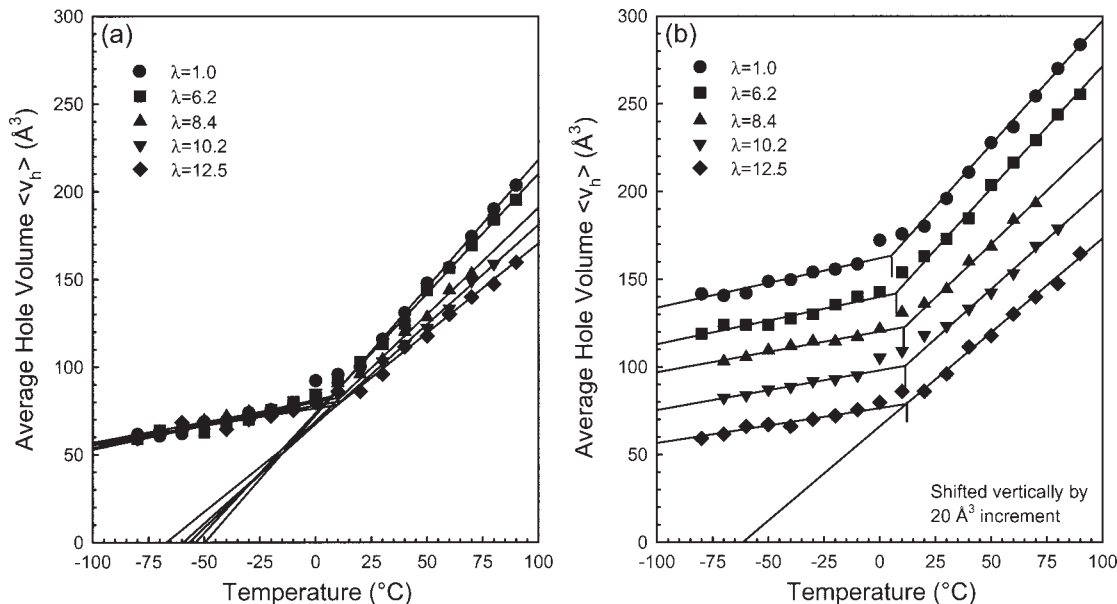


Figure 4. Temperature dependence of $\langle v_h \rangle$ of oriented EP4.5: (a) not shifted and (b) shifted vertically by $20\text{-}\text{\AA}^3$ increments.

tallinity from density at $23\text{ }^\circ\text{C}$ did not change with the orientation, the change in $\alpha_{b,l}$ was attributed to the effect of orientation on the thermal expansivity of the amorphous phase.

The specific volume of the amorphous phase (v_a) above T_g was calculated from the bulk specific volume (v) with ϕ_c from DSC as follows:

$$v_a = \frac{(v - \phi_c v_c)}{(1 - \phi_c)} \quad (4)$$

In the calculation, the specific volume of the crystal (v_c) and the thermal expansivity of the crystal (α_c) were assumed to be those of the polypropylene crystal with $v_c = 1.068\text{ cm}^3\text{ g}^{-1}$ at $23\text{ }^\circ\text{C}$ ²¹ and $\alpha_c = 2.2 \times 10^{-4}\text{ cm}^3\text{ g}^{-1}\text{ K}^{-1}$.²⁰ The amorphous-phase thermal expansivity above T_g ($\alpha_{a,l}$) was obtained as the slope of the linear relationship between v_a and the temperature (T). The amorphous-phase expansivity decreased steadily with the orientation (Table 3).

The decrease in the amorphous-phase thermal expansivity arose from changes in the free-volume structure induced by orientation. Figure 4(a) plots the temperature dependence of the average free-volume hole size ($\langle v_h \rangle$) as determined by PALS for stretched EP4.5 films. For clarity, the data are presented with a constant shift in Figure 4(b). For each material, separate linear fits of the glassy and rubbery regions are shown by solid lines. The intersection of the lines defined T_g . The glass transition obtained in this way increased slightly with λ from $5\text{ }^\circ\text{C}$ for $\lambda = 1.0$ to $12\text{ }^\circ\text{C}$ for $\lambda = 12.5$ (Table 3).

The linear fit for $T > T_g$ was extrapolated to a zero-free-volume hole size at a temperature about $50\text{--}70\text{ }^\circ\text{C}$ below the corresponding T_g . A possible interpretation can be derived from the coincidence of the extrapolated temperature and the postulated second-order transition T_2 at about $T_g - 60\text{ }^\circ\text{C}$.^{22–24} The thermal expansivity of free-volume holes was much smaller below T_g than above T_g but decreased similarly with orientation. For comparison, the thermal expansivity of the free-volume holes in the glassy state decreased from $0.27\text{ }^\circ\text{K}^{-1}$ for $\lambda = 1$ to $0.20\text{ }^\circ\text{K}^{-1}$ for $\lambda = 12.5$, whereas in the rubbery state the expansivity decreased from 1.46 to $1.04\text{ }^\circ\text{K}^{-1}$ for the same λ values.

The free-volume hole size taken together with the free-volume hole density (N_h ; g^{-1}) defines the specific hole free volume of the amorphous phase (v_f ; $\text{cm}^3\text{ g}^{-1}$) as follows:

$$v_f = N_h \langle v_h \rangle \quad (5)$$

where $\langle v_h \rangle$ is the mean free-volume hole size (cm^3). It follows that the fractional free volume (FFV) of the amorphous phase can be calculated as follows:

$$\text{FFV} = \frac{v_f}{v_a} \quad (6)$$

The hole density can be obtained if we consider v_a to be the sum of the specific occupied

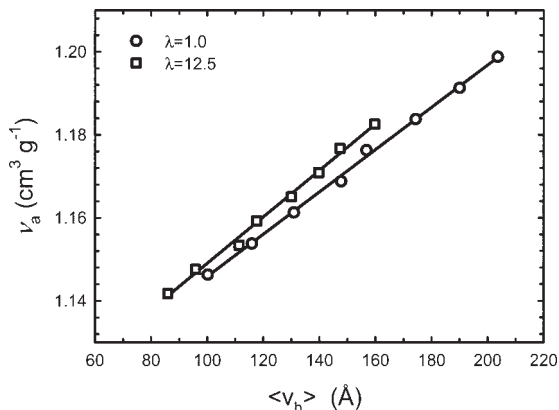


Figure 5. Correlation between $\langle v_h \rangle$ and v_a .

volume (v_{occ}) and the specific hole free volume:²⁵

$$v_a = v_{occ} + \langle v_h \rangle N_h \quad (7)$$

It has been suggested that N_h is constant and independent of temperature; that is, an increasing specific volume arises from the expansion of existing free-volume holes and not by the formation of new holes. An excellent linear correlation of v_a versus $\langle v_h \rangle$ for $T > T_g$, as illustrated in Figure 5 for $\lambda = 1$ and $\lambda = 12.5$, indicated that the hole density indeed was independent of temperature. Furthermore, the same hole density was assumed to persist below T_g because the excess holes in the glassy state arise from the freezing of the free-volume holes that are mobile above T_g . The hole density extracted from the slope increased somewhat with orientation from $5.1 \times 10^{20} \text{ g}^{-1}$ for $\lambda = 1$ to $5.6 \times 10^{20} \text{ g}^{-1}$ for $\lambda = 12.5$ (Table 3). The magnitude of the hole density was consistent with previous findings for other polymers.^{25–28}

Oxygen-Transport Properties

Typical experimental oxygen flux curves in Figure 6 describe the oxygen flux through films of 190- μm heat-set control films at temperatures above and below T_g . The initial increase in the oxygen flux reflected non-steady-state diffusion. This part of the curve was determined by the diffusivity. The steady-state flux was determined by the permeability. The temperature had a strong effect on both the non-steady-state and steady-state regions. Reducing the temperature

broadened the non-steady-state region (lower diffusivity) and dramatically decreased the steady-state flux (lower permeability). To obtain diffusivity D and to accurately determine permeability P , the data were fit to the solution of Fick's second law with appropriate boundary conditions:²⁹

$$J(t) = \frac{Pp}{l} \left[1 + 2 \sum_{n=1}^{\infty} (-1)^n \exp\left(-\frac{D\pi^2 n^2 t}{l^2}\right) \right] \quad (8)$$

where $J(t)$ is the oxygen flux. The fitting curves are included with the experimental points in Figure 6 with two fitting parameters; Pl^{-1} and Dl^{-2} . With the average film thickness, P and D were determined within 3% error. Solubility S was obtained from the relationship $S = PD^{-1}$. The oxygen-transport properties at 23 and -30 °C are summarized in Table 1.

The value of P for an unoriented EP4.5 640- μm film at 23 °C, $9.15 \text{ cc(STP) cm m}^{-2} \text{ day}^{-1} \text{ atm}^{-1}$, was somewhat higher than P reported in the literature for isotactic polypropylene homopolymer, $6.8 \text{ cc(STP) cm m}^{-2} \text{ day}^{-1} \text{ atm}^{-1}$.⁴ This difference was reasonable because of the lower crystallinity of the copolymer in comparison with that of the isotactic homopolymer. The values of D and S at 23 °C were also comparable to the reported values for polypropylene.³⁰ The change in the slope of the logarithmic dependence of P on T^{-1} defined the glass transition at -7 °C (Fig. 7), which was very close to the T_g value determined by dynamic mechanical thermal analysis at 1 Hz of -5 °C. The increase in P by a factor of about 120 from $0.28 \text{ cc(STP) cm m}^{-2} \text{ day}^{-1} \text{ atm}^{-1}$ at -35 °C to $34 \text{ cc(STP) cm m}^{-2} \text{ day}^{-1} \text{ atm}^{-1}$ at 45 °C was primarily due to an increase in D .

Unoriented films of different thicknesses exhibited essentially the same temperature-dependent values of P , which were obtained from the steady-state flux (Fig. 7). However, with highly permeable polymer films such as EP4.5, the film thickness was critical to resolving the non-steady-state region of the flux curve from which D was obtained. If the temperature was below -10 °C when D was small, the same temperature dependence in D and S was obtained for all film thicknesses. However, above -10 °C, the diffusivity obtained by the fitting of the initial portion of the flux curve of the thinner 110- μm film deviated from the value obtained for the thicker 640- μm film. The apparent temperature independence of

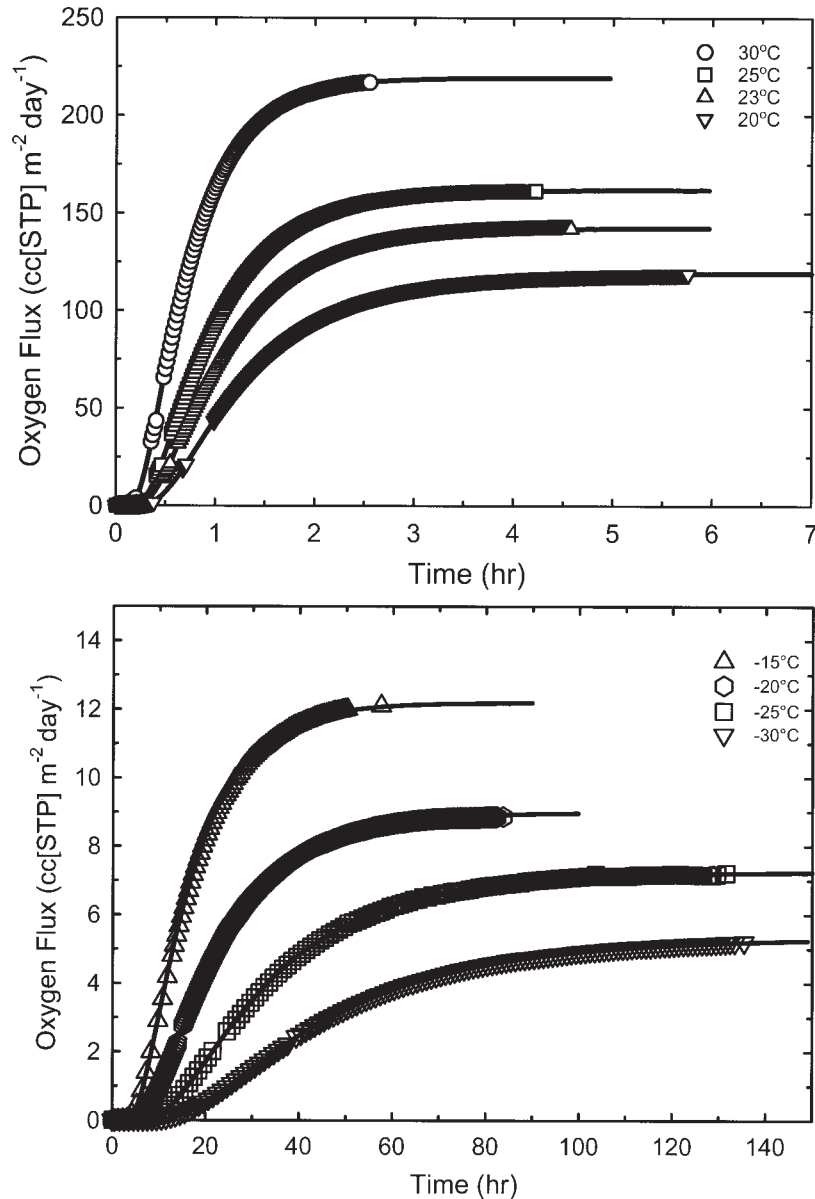


Figure 6. Experimental oxygen flux data and fit to the solution of Fick's second law (solid lines) for unoriented EP4.5 films at various temperatures above and below T_g .

D reflected the time response limit of the oxygen sensor. Correspondingly, the apparent solubility increased to realistically high values.

The time to reach equilibrium flux (t_0) for a film of thickness l is related to D as follows:³¹

$$t_0 = \frac{l^2}{6D} \quad (9)$$

The characteristic response time of the Mocon oxygen detector required t_0 to be larger than 0.8 h to obtain diffusivity reliably. For 110- and 190- μm EP4.5 films, D and hence S could be obtained reli-

ably below T_g only, that is, -10 to -35 $^\circ\text{C}$. This limitation also applied to D and S of oriented EP4.5 films, which had thicknesses of 110–210 μm .

The temperature dependence of the permeability for oriented films is plotted in Figure 8. Orientation resulted in decreased permeability of both glassy and rubbery states. The T_g values obtained from the change in the slope of the logarithmic dependence of P on T^{-1} increased with orientation from -7 to 4 $^\circ\text{C}$. The increase in T_g determined by oxygen permeability paralleled the increase in T_g determined by PALS.

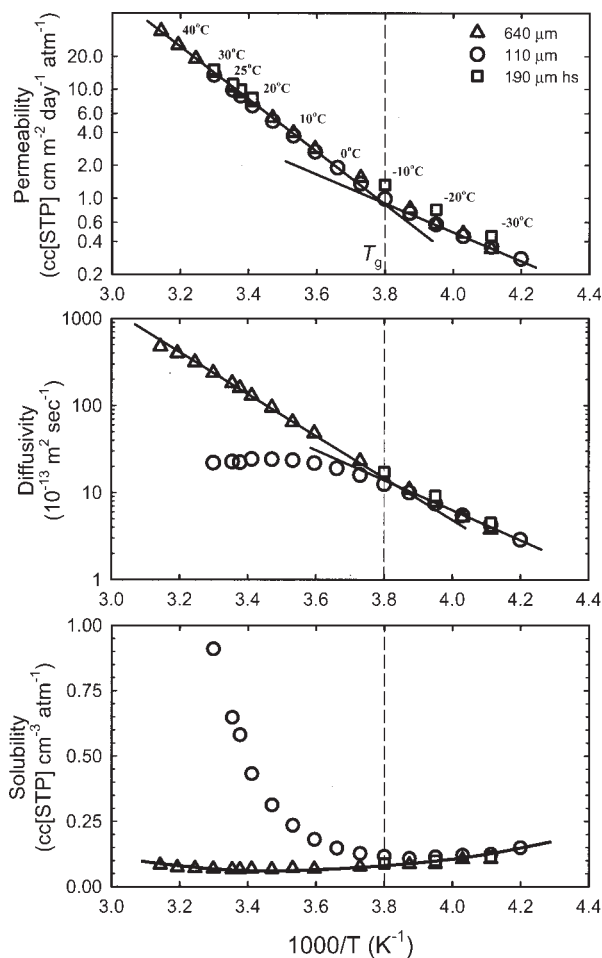


Figure 7. Temperature dependence of P , D , and S for unoriented EP4.5 films of different thicknesses.

The oxygen permeability at 23 °C is plotted as a function of λ in Figure 9 with additional data points included. Orientation to a λ value of about 6 had only a small effect on P . However, P decreased by a factor of almost 3, from 9.14 to 3.4 cc(STP) cm m⁻² day⁻¹ atm⁻¹, as λ increased from 6.8 to 12.5 (Table 2).

The effect of λ on the oxygen permeability, diffusivity, and solubility below T_g is illustrated in Figure 10 with data obtained at -30 °C. Although P was much smaller below T_g than above, the effect of λ persisted at the lower temperature with decreasing P , beginning at a λ value of about 6. The effect of λ on P was primarily due to the effect on the diffusivity. The solubility showed small variations but no consistent trend with increasing λ .

The energetic parameters for permeability and diffusivity were obtained by the plotting of

the temperature dependence of P and D according to the following relationships:

$$D = D_0 \exp\left(-\frac{E_D}{RT}\right) \quad (10)$$

$$P = P_0 \exp\left(-\frac{E_P}{RT}\right) \quad (11)$$

Values of the activation energy for permeability (E_P) and the activation energy for diffusion (E_D) and the prefactors $\ln P_0$ and $\ln D_0$ are summarized in Table 4. Above T_g , E_P and $\ln P_0$ decreased systematically with increasing λ . Below T_g , an effect of orientation on E_P and $\ln P_0$ was less apparent; indeed, it appeared that both quantities decreased at a λ value of about 6 in comparison with those of the unoriented control, but they gradually increased at higher λ values.

The energetic parameters for diffusion were obtained only below T_g . Both E_D and $\ln D_0$ appeared to decrease with orientation. A plot of $\ln D_0$ versus E_D showed that the linear free energy rule, which is observed for many glassy polymers, also holds for drawn EP4.5 (Fig. 11). The slope of 5×10^{-4} m² mol s⁻¹ J⁻¹ is consistent with literature reports, which range from 3.2 to 11×10^{-4} m² mol s⁻¹ J⁻¹ for various simple gases in a wide variety of polymers.³²⁻³⁴

DISCUSSION

Oxygen Sorption

The impermeability of crystals is the basis of the simple two-phase solubility model, which consists of an impermeable crystalline phase dispersed in a permeable amorphous matrix. The resulting relationship between the bulk solubility (S) and ϕ_c is

$$S = S_a(1 - \phi_c) \quad (12)$$

where S_a is the solubility of the gas in the amorphous phase. The application of eq 12 generally assumes that S_a is constant and that S depends only on ϕ_c . If orientation affects the density of the amorphous phase, the assumption of constant S_a may not be valid.^{7,8} However, in the case of oriented EP4.5, the crystallinity, bulk density and therefore ρ_a at 23 °C are essentially unchanged by orientation. Thus, S_a should be constant, and S should not change with λ .

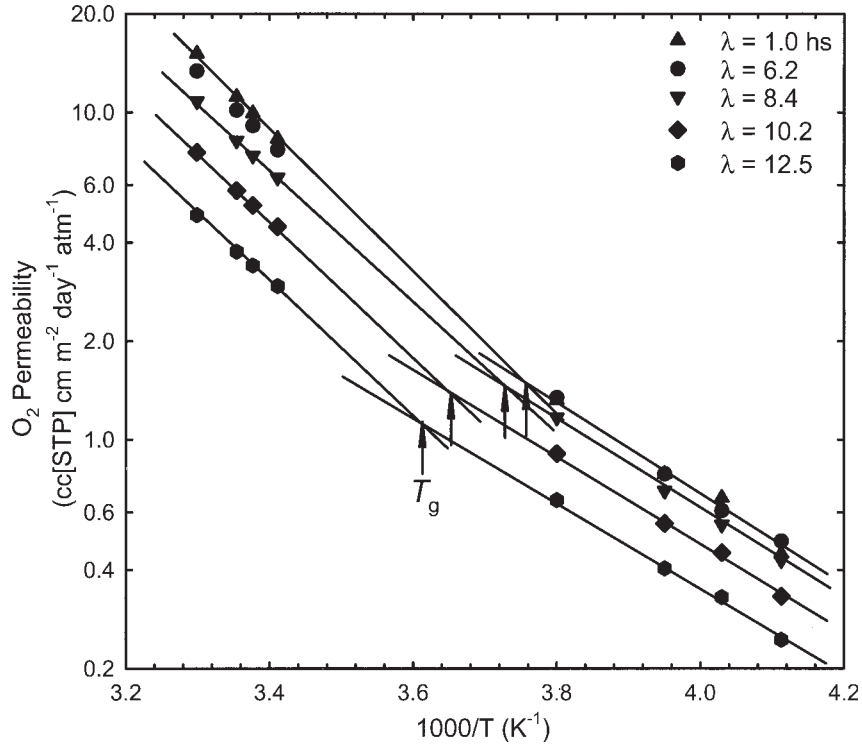


Figure 8. Temperature dependence of the oxygen permeability of oriented EP4.5 films.

Reliable values of D and S were obtained only below T_g between -10 and -35 °C when D was small enough that the condition described by eq 9 was met. However, below T_g where S could be obtained, the oxygen solubility scattered somewhat but showed no systematic trend with λ . The corresponding value of S_a was about 0.21 cc(STP) cm^{-3} atm^{-1} at -30 °C (Table 3).

Gas solubility in a glassy polymer at a low pressure is the process of filling free-volume holes of the amorphous phase.^{7,8} A constant S_a value below T_g , independent of λ , should be reflected as a constant excess-hole free volume. In fact, FFV of EP4.5, calculated independently from the hole size and hole density at -30 °C according to eqs 5 and 6, was 0.033 over the range of λ values examined (Table 3). Gradually increasing N_h was offset by a gradually decreasing free-volume hole size.

Proportionality between S_a and v_f in the glassy state is expressed as follows:^{7,8,35}

$$S_a = \beta v_f \quad (13)$$

where β indicates the physical state of sorbed oxygen in the free-volume holes at a given pressure and temperature. With average values of v_f from eq 5 and S_a from eq 12, β was 5.4 cc(STP) g cm^{-6} atm^{-1} at -30 °C, which was slightly higher than the β

value obtained at the ambient temperature for various glassy polyesters, 3.6 cc(STP) g cm^{-6} atm^{-1} .⁷ From β , the sorbed oxygen density (ρ_{O_2}) in the static free-volume holes can be obtained as follows:

$$\rho_{O_2} = \frac{v_a \beta p M_w}{22,400} \quad (14)$$

where v_a is the specific volume of the glassy phase, $p = 1$ atm is the ambient pressure of oxygen gas,

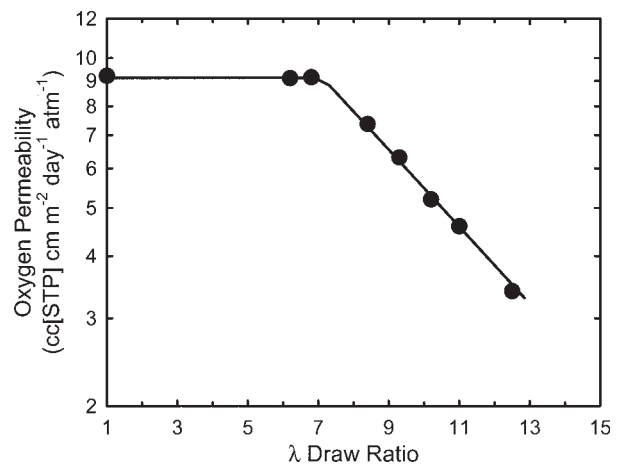


Figure 9. Effect of λ on the oxygen permeability of EP4.5 films at 23 °C.

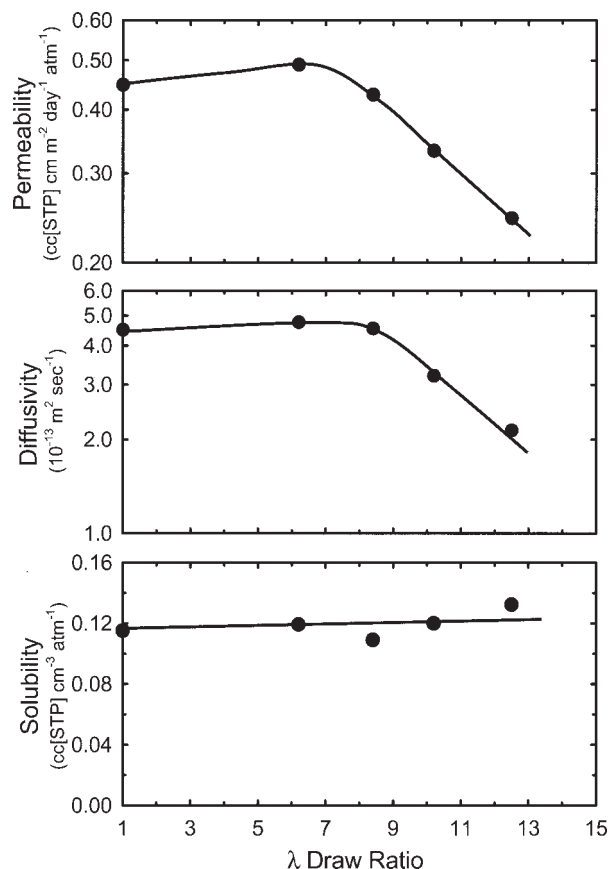


Figure 10. Effect of λ on P , D , and S for oriented EP4.5 films at $-30\text{ }^{\circ}\text{C}$.

and $M_w = 32$ is the molecular weight for oxygen. ρ_{O_2} , about $8.5 \times 10^{-3}\text{ g/cm}^3$ of free volume or about 5 atm at $-30\text{ }^{\circ}\text{C}$, indicates that the sorbed oxygen is in the gaseous state. This compares with the pressure of sorbed oxygen in glassy polyesters of about 3 atm under ambient conditions ($23\text{ }^{\circ}\text{C}$ and 1 atm).^{7,35}

Oxygen Diffusivity

The decrease in P below T_g as λ increases from 6 to 12 is primarily due to decreasing D . It seems reasonable to assume that the similar drop in P above T_g is also due to decreasing D (Fig. 10). Although reduced free volume could contribute to the decrease in D , this seems unlikely because of the essentially constant density (Table 2) and constant FFV from PALS at $23\text{ }^{\circ}\text{C}$ (Table 3). Others have also observed that little if any density change occurs in stretched polypropylene.^{4,36} Therefore, the drop in the diffusivity as λ increases from 6 to 12 cannot be attributed to a decrease in the free volume but

must be attributed to a change in the amorphous structure.

It has been suggested that with λ increasing from 1 to 6, lamellar breakup and reorganization occur without significant orientation of the amorphous phase.¹⁹ As the microfibrils become fully developed, orientation of the amorphous phase at higher λ values is associated with an increasing number of taut tie chains. As a result, the amorphous chain mobility is gradually reduced with increasing λ . In this study, evidence of reduced amorphous chain mobility is indicated by an increase in T_g , as observed in both PALS and oxygen permeability (Table 3). Reduced amorphous chain mobility also accounts for decreasing bulk amorphous-phase thermal expansivity from density and a reduction in the thermal expansivity of free-volume holes from PALS.

The amorphous chain mobility is a determining factor in the dynamic component of free volume, which determines gas diffusivity.³⁵ Following the interpretation proposed by others,¹¹ we find it reasonable to attribute decreasing diffusivity at higher λ values to an increasing number of taut tie molecules. The interpretation of diffusivity in terms of static and dynamic free-volume concepts leads to a very simple lattice model for oxygen transport in the glassy state.^{8,37} In this discussion, it is assumed that the tortuosity factor imposed by the crystalline phase does not change significantly after fibril formation at a λ value of about 6. This is reasonable in terms of the deformation model, which attributes structural changes between λ values of 6 and 12 primarily to the amorphous phase. Spherical free-volume holes having radius r are assumed to be arranged on a cubic lattice. The concept is similar to lattice models previously used to describe both the rubbery and glassy states.^{38,39} The average distance between neighboring holes is estimated from a mechanistic interpretation of E_D ;⁴⁰⁻⁴³ the energy required to create a channel of cross-sectional area $\pi d^2/4$ and jump length α is equated with the energy required to break the physical bonds between the polymer segments:

$$E_D = \frac{1}{4} \pi d^2 \alpha C E_D N_A \quad (15)$$

where d is the collision diameter of the gas penetrant, CED is the cohesive energy density of the polymer determined by a group contribution method,⁴⁴ N_A is Avogadro's number, and E_D is

Table 4. Energetic Parameters of Oriented EP4.5 Films

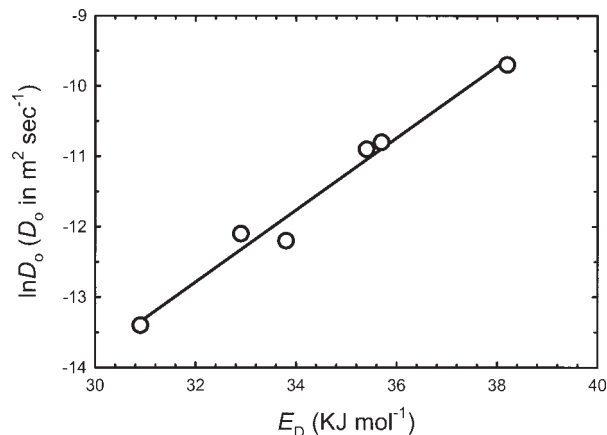
λ	$\ln P_0^a$	E_P (kJ mol ⁻¹)	$\ln D_0$ (D_0 in m ² s ⁻¹)	E_D (kJ mol ⁻¹)	α (nm)
Below T_g					
1.0 (640 μm)	12.5	27.3	-9.7	38.2	2.4
1.0 (190 μm , heat-set)	13.4	28.8	-10.8	35.7	2.2
6.2	11.2	24.2	-10.9	35.4	2.2
8.4	11.5	25.0	-12.1	32.9	2.1
10.2	11.5	26.1	-12.2	33.8	2.1
12.5	12.1	26.7	-13.4	30.9	1.9
Above T_g					
1.0 (640 μm)	20.6	45.3	-6.8	44.5	—
1.0 (190 μm , heat-set)	20.3	44.3	—	—	—
6.2	18.8	41.0	—	—	—
8.4	18.2	39.8	—	—	—
10.2	17.4	38.9	—	—	—
12.5	16.2	37.0	—	—	—

^a P_0 in cc[STP] cm m⁻² day⁻¹ atm⁻¹.

determined by the Arrhenius relationship between $\ln D$ and T^{-1} . According to the concept expressed by eq 15, decreasing activation energy for oxygen diffusion through oriented EP4.5 translates to a decrease in the diffusional jump length from 2.2 to 1.9 nm between λ values of 6.2 and 12.5 (Table 4). This decrease with orientation qualitatively conforms with the observed increase in the hole density from PALS (Table 3).

The decrease in α alone does not account for the observed decrease in D from 4.76 to 2.14 $\times 10^{-13}$ m² s⁻¹ (Table 3). In addition to α , the amorphous diffusivity (D) also depends on the effective jump frequency (ω) as follows:⁴⁵

$$D \propto \omega \alpha^2 \quad (16)$$

**Figure 11.** Linear relationship between $\ln D_0$ and E_D .

It follows that the orientation of EP4.5 decreases ω . At -30 °C, for example, the observed reduction in D between λ values of 6 and 12 requires that ω decrease by 40%. A decrease in ω is consistent with an increasing number of taut tie molecules, which reduce amorphous chain mobility and as a result, reduce accessible segmental relaxations available for oxygen diffusion.^{35,46}

CONCLUSIONS

This study of a propylene copolymer (EP4.5) reveals that stretching to a λ value of about 6 has almost no effect on oxygen permeability. Only higher λ values result in decreased permeability. This may be general behavior of propylene-based polymers as a similar trend has been reported for isotactic propylene homopolymer.¹¹ The effect of orientation is qualitatively the same, regardless of whether the amorphous phase is in the rubbery or glassy state, even though the mechanism of oxygen transport may differ as indicated by higher activation energy for oxygen permeability above T_g .

Changes in permeability are due to changes in diffusivity; oxygen solubility remains essentially unaffected by orientation. The oxygen-transport results are interpreted in terms of static and dynamic components of the amorphous-phase free volume. Orientation appears to have relatively little effect on the total static free volume. This is inferred from essentially constant oxygen

solubility and constant crystallinity, as determined from DSC and bulk density, and is confirmed by the direct probing of the free volume with PALS. A slight increase in N_h is offset by a decrease in the hole size. The sorbed oxygen is in the gaseous state with a pressure of approximately 5 atm at -30°C .

Decreased diffusivity is attributed to structural changes in the amorphous phase that occur during strain hardening and their effect on the dynamic component of the free volume. The later stages of microfibril development are accompanied by an increasing number of taut tie chains. The resulting reduction in the amorphous chain mobility is reflected as a higher T_g of drawn films and a lower bulk thermal expansivity of the amorphous phase. The latter effect correlates with a decrease in the thermal expansivity of free-volume holes from PALS. Decreased diffusivity in the glassy state of oriented EP4.5 can be attributed to a reduction in both the diffusional jump length and jump frequency.

This research was generously supported by Applied Extrusion Technologies, Inc. Support from Modern Controls, Inc., for the development of a facility for gas-transport studies at Case Western Reserve University is gratefully acknowledged.

REFERENCES AND NOTES

- Paul, D. R.; Clarke, R. *J Membr Sci* 2002, 208, 269–283.
- Benning J. *Plastic Films for Packaging*; Technomic: Lancaster, PA, 1983; pp 37–43.
- Bur J.; Roth, S. C. *Polym Eng Sci*, 2004, 44, 805–813.
- Taraiya K.; Orchard, G. A. J.; Ward, I. M. *J Appl Polym Sci*, 1990, 41, 1659–1671.
- Karacan I.; Taraiya, A. K.; Bower, D. I.; Ward, I. M. *Polymer*, 1993, 34, 2691–2701.
- Taraiya, A. K.; Orchard, G. A. J.; Ward, I. M. *Plast Rubber Compos Process Appl*, 1993, 19, 273–278.
- Liu, R. Y. F.; Schiraldi, D. A.; Hiltner, A.; Baer, E. *J Polym Sci Part B: Polym Phys*, 2002, 40, 862–877.
- Liu, Y. F.; Hiltner, A.; Baer, E. *J Polym Sci Part B: Polym Phys*, 2004, 42, 493–504.
- Slee, J. A.; Orchard, G. A. J.; Bower, D. I.; Ward, I. M. *J Polym Sci Part B: Polym Phys*, 1989, 27, 71–83.
- Petelin, A. *Colloid Polym Sci*, 1987, 265, 357–382.
- Vittoria, V.; De Candia, F.; Capodanno, V.; Peterlin, A. *J Polym Sci Part B: Polym Phys*, 1986, 24, 1009–1019.
- Higuchi, H.; Yu, Z.; Jamieson, A. M.; Simha, R.; McGervey, J. D. *J Polym Sci Part B: Polym Phys*, 1995, 33, 2295–2305.
- Natale, R.; Russo, R.; Vittoria, V. *J Mater Sci*, 1992, 27, 4350–4354.
- Krigbaum, W. R.; Uematsu, W. R. *J Polym Sci Part A: Gen Pap*, 1965, 3, 767–776.
- Hai-Shan, B.; Cheng S. Z. D.; Wunderlich, B. *Makromol Chem Rapid Commun*, 1988, 9, 75–77.
- Isasi, J. R.; Mandelkern, L.; Galante, M. J.; Alamo, R. G. *J Polym Sci Part B: Polym Phys*, 1999, 37, 323–334.
- Lin, X. D.; Jia, D.; Leung, F. K. P.; Cheung, W. L. *J Appl Polym Sci*, 2004, 93, 1989–2000.
- Galeski, A. *Prog Polym Sci*, 2003, 28, 1643–1699.
- Samuels, R. J. *J Polym Sci Part A-2: Polym Phys*, 1978, 6, 1101–1139.
- Van Krevelen W. *Properties of Polymers*, 3rd ed.; Elsevier: Amsterdam, 1997; Chapter 4.
- Brandrup, J.; Immergut, E. H. *Polymer Handbook*, 3rd ed.; Wiley: New York, 1989; Section V, p 27.
- Gibbs, J. H.; DiMarzio, E. A. *J Chem Phys*, 1958, 28, 373–383.
- Miller, A. A. *J Polym Sci Part A: Gen Pap*, 1963, 1, 1857–1863.
- Miller, A. A. *J Polym Sci Part A: Gen Pap*, 1963, 1, 1865–1874.
- Srtithawatpong, R.; Peng, Z. L.; Olson, B. G.; Jamieson, A. M.; Simha, R.; McGervey, J. D.; Maier, T. R.; Halasa, A. F.; Ishida, H. *J Polym Sci Part B: Polym Phys*, 1999, 37, 2754–2770.
- Dlubek, G.; Bondarenko, V.; Pionteck, J.; Supej, M.; Wutzler, A.; Krause-Rehberg, R. *Polymer*, 2003, 44, 1921–1926.
- Bamford, D.; Dlubek, G.; Reiche, A.; Alam, M. A.; Meyer, W.; Galvosas, P.; Rittig, F. *J Chem Phys*, 2001, 115, 7260–7270.
- Hong, X.; Jean, Y. C.; Yang, H. J.; Jordan, S. S.; Koros, W. J. *Macromolecules*, 1996, 29, 7859–7864.
- Sekelik, D. J.; Stepanov, E. V.; Nazarenko, S.; Schiraldi, D. A.; Hiltner, A.; Baer, E. *J Polym Sci Part B: Polym Phys*, 1999, 37, 847–857.
- Van Krevelen D. W. *Properties of Polymers*, 3rd ed.; Elsevier: Amsterdam, 1997; Chapter 18.
- Vieth, W. R. *Diffusion in and through Polymers: Principles and Applications*; Hanser: Munich, 1991.
- Hu, Y. S.; Liu, R. Y. F.; Schiraldi, D. A.; Hiltner, A.; Baer, E. *Macromolecules*, 2004, 37, 2136–2143.
- Van Amerongen G. J. *J Appl Phys*, 1946, 17, 972.
- Barrer, R. M.; Skirrow, G. *J Polym Sci*, 1948, 3, 549–563.
- Polyakova, A.; Liu, R. Y. F.; Schiraldi, D. A.; Hiltner, A.; Baer, E. *J Polym Sci Part B: Polym Phys*, 2001, 39, 1889–1899.
- de Candia F.; Perullo, A.; Vittoria, V.; Peterlin, A. In *Interrelations between Processing Structure*

- and Properties of Polymeric Materials; Seferis, J. C.; Theocaris, P. S., Eds.; Materials Science Monographs 21; Elsevier: Amsterdam, 1984; p 713.
37. Hu, Y. S.; Liu, R. Y. F.; Schiraldi, D. A.; Hiltner, A.; Baer, E. *Macromolecules*, 2004, 37, 2136–2143.
 38. Rane, S.; Gujrati, P. D. *Phys Rev E*, 2001, 64, 011801.
 39. Simha, R.; Somcynsky, T. *Macromolecules*, 1969, 2, 342–350.
 40. Meares, P. *J Am Chem Soc*, 1954, 76, 3415–3422.
 41. Thran, A.; Kroll, G.; Faupel, F. *J Polym Sci Part B: Polym Phys*, 1999, 37, 3344–3358.
 42. Duda, J. L.; Zielinski, J. M. In *Diffusion in Polymers*; Neogi, P., Ed.; Marcel Dekker: New York, 1996; p 143.
 43. Takeuchi, H. *J Chem Phys*, 1990, 93, 2062–2067.
 44. Van Krevelen D. W. *Properties of Polymers*, 3rd ed.; Elsevier: Amsterdam, 1997; Chapter 7.
 45. Petropoulos, J. H. In *Polymeric Gas Separation Membranes*; Paul, D. R.; Yampol'ski, Y. P., Eds.; CRC: Boca Raton, 1994; p 17.
 46. Andrade, G. S.; Collard, D. M.; Schiraldi, D. A.; Hu, Y. S.; Baer, E.; Hiltner, A. *J Appl Polym Sci*, 2003, 89, 934–942.